Available online at www.sciencedirect.com
ScienceDirect
Physica C 468 (2008) 464–470
PHYSICA C
www.elsevier.com/locate/physc

Thermodynamic properties of the clathrate-type silver-oxide $Ag_6O_8AgHF_2$

K. Kawashima [a,*], M. Kriener [b], M. Ishii [a], Y. Maeno [b], J. Akimitsu [a]

[a] Department of Physics and Mathematics, Aoyama-Gakuin University, Kanagawa 229-8558, Japan
[b] Department of Physics, Graduate School of Science, Kyoto University, Kyoto 606-8502, Japan

Received 10 December 2007; received in revised form 25 January 2008; accepted 30 January 2008
Available online 8 February 2008

Abstract

We report normal-state and superconducting properties of the clathrate-type silver-oxide $Ag_6O_8AgHF_2$. We present electrical resistivity, DC- and AC-susceptibility and specific-heat measurements of single crystalline $Ag_6O_8AgHF_2$. In the normal state, $Ag_6O_8AgHF_2$ exhibits metallic conductivity and a phase transition near 110 K, possibly a structural phase transition as observed in the related compound $Ag_6O_8AgNO_3$. The onset of superconductivity of our samples is observed around 1.2–1.5 K, and the H–T phase diagram is determined for the first time. The upper critical field $H_{c2}(0)$ is estimated to be about 2000–2200 Oe and the coherence length $\xi_{GL}(0)$ to be 40 nm.

PACS: 74.70.−b; 74.25.Ha; 74.25.Jb

Keywords: Clathrate-type; Silver-oxide; Resistivity; AC susceptibility; Specific heat; $Ag_6O_8AgHF_2$

1. Introduction

We report here a silver-oxide superconductor which belongs to the family of silver clathrates Ag_6O_8MX (M = cation, X = anion) with M = Ag. For X = NO_3^-, BF_4^-, and HF_2^-, superconductivity was already reported in the 1960s with critical temperatures $T_c = 1.0$ K, 0.15 K, and 1.0–1.5 K, respectively [1–3]. For other family members with X = HSO_4, HCO_3, or in more general for M = Tl or Hg, $Ag_6O_8TlClO_4$, and $Ag_6O_8HgClO_4$, only the synthesizing methods and crystal-structure analyses have been reported so far [4–7].

At room temperature, Ag_6O_8MX crystallizes in a cubic structure, space group $Fm\bar{3}m$ (No. 225). The Ag, O, M, and X ions occupy the 24d, 32f, 4b, and 4a Wyckoff positions, respectively [8–11]. A unique structural feature throughout the whole Ag_6O_8MX family is the location of the X anions in the centers of oversized Ag_6O_8 cages. The M ions are located in the cuboid-like spaces between the Ag_6O_8 cages as shown in Fig. 1. The surface of the Ag_6O_8 cage consists of square planar AgO_4 units which resemble the CuO_4 structural element realized in the high-T_c cuprates. The chemical composition of the Ag_6O_8 cages forces the Ag ions partly to realize an unusual high valency such as Ag^{2+} or even Ag^{3+}. The reason for the existence of different Ag valences is the fractional formal Ag ion valence in the Ag_6O_8 cages, i.e., +2.67. The family of Ag_6O_8MX compounds are, therefore, a class of interesting materials with the Ag_6O_8 cages as characteristic structural element. However, the nature of the superconducting state is not well understood. In order to obtain more information on the superconducting ground state of Ag_6O_8MX, we investigated the compounds with M = Ag and X = NO_3^- (Ref. [13]) and HF_2^-. In this paper we focus on

* Corresponding author. Tel.: +81 42 759 6545; fax: +81 42 759 6287.
E-mail address: kawaken@phys.aoyama.ac.jp (K. Kawashima).

0921-4534/$ - see front matter © 2008 Elsevier B.V. All rights reserved.
doi:10.1016/j.physc.2008.01.008

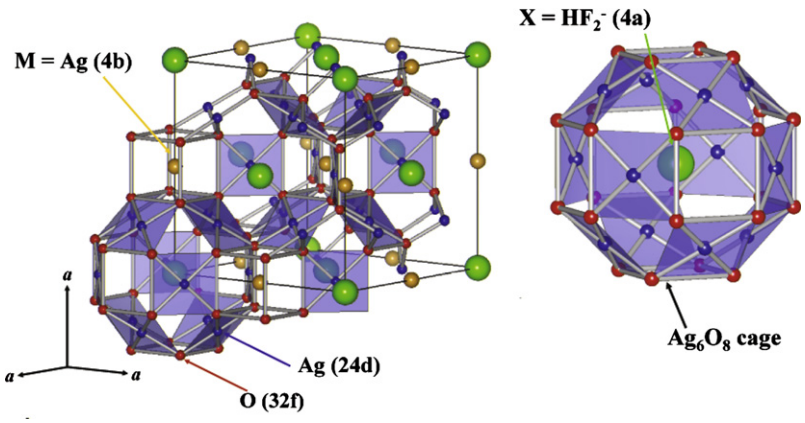

Fig. 1. Crystal structure of $Ag_6O_8AgHF_2$: The solid lines in the left figure mark the unit cell. The right drawing gives an enlarged view of the characteristic Ag_6O_8 cage with the X anion in its center. (The program VESTA is used [12].)

$Ag_6O_8AgHF_2$, which is to our knowledge the material which exhibits the highest-T_c value so far reported among the whole family of Ag_6O_8MX silver clathrates.

There are only two early publications dealing with $Ag_6O_8AgHF_2$ available: by Gossard et al. (Ref. [2], published in 1967) and by Conway et al. (Ref. [3], 1970). The former one reported superconductivity in $Ag_6O_8AgHF_2$ with T_c values of about 1.0–1.5 K. The latter publication reported the temperature dependence of the specific heat in the superconducting state. However, the specific-heat data in Ref. [3] exhibit a very broad superconducting transition. The authors explained this broadness due to paramagnetic impurities contained in their samples. Therefore, they did not carry out any further analysis of their data. Thus, the superconducting properties, e.g. the coherence length, the upper critical field, or the H–T phase diagram of $Ag_6O_8AgHF_2$ are still unknown. In order to examine the superconducting phase of $Ag_6O_8AgHF_2$ and also to obtain information on the normal-state properties, single crystalline samples are desirable.

In this paper, we present the results of electrical resistivity ρ, specific heat C_P, and DC- and AC-susceptibility (χ_{DC} and χ_{AC}) measurements using newly-prepared single-crystalline samples of $Ag_6O_8AgHF_2$. We estimate the basic physical quantities in the superconducting state and discuss the superconducting properties in a Ginzburg–Landau framework. We newly present the H–T phase diagram of $Ag_6O_8AgHF_2$. Finally, we discuss the superconducting state in Ag_6O_8MX and compare the results on $Ag_6O_8AgHF_2$ (this work) with those on $Ag_6O_8AgNO_3$ (reported in Ref. [13]).

2. Experimental details

$Ag_6O_8AgHF_2$ samples were synthesized by an electrochemical reaction using HF solution [14]. We used 99.99%-AgF powder and 3–10% concentrated HF solution as starting materials. We dissolved 40 g AgF powder in 100 ml HF solution. For the electrochemical reaction a platinum plate (anode) and platinum wire (cathode) were used. The synthesis current was supplied by a stabilized power supply with a maximum current of 1.0 A. The samples, which grew at the anode, were washed with cold-distilled water and dried in vacuum. The needle-like samples are black/grey colored with a typical length of several millimeters.

Some specimens of Ag_6O_8MX were reported to loose oxygen if exposed to air [10]. From our experience, moisture is also a crucial parameter. Especially for $Ag_6O_8AgHF_2$, we observed a surface deterioration of the samples if they were kept on air too long. To avoid a possible damage of the samples, we kept them in dry Ar atmosphere except the time when a sample was mounted to an experimental setup prior to a measurement.

We confirmed by powder X-ray diffraction that the synthesized phase is indexed as a cubic unit cell, space group $Fm\bar{3}m$. We did not detect any impurity phases. Moreover, we checked that the samples are single crystalline by taking X-ray Laue patterns.

The electrical resistivity was measured by a conventional four-probe method applying a DC current of 0.1 mA using a commercial setup (Quantum Design, PPMS) between 0.4 K and 300 K. The DC magnetization measurement was performed using a commercial SQUID magnetometer (Quantum Design, MPMSR2) in the temperature range $2\ K \leqslant T \leqslant 300\ K$. The AC susceptibility measurements down to 0.3 K were performed with a ^{3}He refrigerator (Oxford Instruments, Heliox) inserted into a standard superconducting magnet by a mutual-inductance method. In order to avoid heating effects during the low-T measurements, a small AC field of 83 mOe-rms was chosen. The frequency of the AC field was 3011 Hz. The temperature dependence of the in-field susceptibility data was taken as follows: The external DC magnetic field was set above T_c. Then the temperature was reduced down to about 300 mK (field-cooling (FC) run) and subsequently increased above T_c (warming after FC run). The specific-heat measurements were performed applying a relaxation-time method using a commercial calorimeter (Quantum Design, PPMS) between 0.4 K and 300 K.

3. Experimental results and discussion

3.1. Normal state properties

Fig. 2 shows the temperature dependence of (a) electrical resistivity ρ, (b) specific heat C_P, and (c) DC susceptibility $\chi_{DC} = M/H$ for $T_c \leqslant T \leqslant 300$ K. The resistivity exhibits a metallic temperature dependence in the whole temperature interval above T_c. In the temperature range between approximately 50 K and 100 K, the resistivity is proportional to T^2. Below 50 K, this changes gradually toward a T^3 behavior in the temperature interval 2 K $< T <$ 30 K. The resistivity at 300 K amounts to ~450 μΩ cm, and the residual resistivity ratio $\rho_{300\ K}/\rho_{0\ K}$ is 15. The resistivity data exhibits a slope change near 110 K which is clearly visible in the derivative $d\rho/dT$ given in the inset of Fig. 2a. The anomaly is also reflected in the specific-heat data, which exhibits a clear jump-like anomaly at that temperature, and in the DC susceptibility, which features a kink near 110 K as indicated by the dashed line in Fig. 2. However, the origin of these anomalies remains unclear. The related compound $Ag_6O_8AgNO_3$ undergoes a structural phase transition at 185 K causing similar anomalies in $\rho(T)$, $C_P(T)$, and $\chi_{DC}(T)$, which could also be the case in $Ag_6O_8AgHF_2$. Gossard et al. [2] reported a small anomaly in their resistivity data around 220 K. We note that we do not find any indication of this anomaly in our data. The dip visible in C_P around this temperature in Fig. 2b is most probably an experimental artifact.

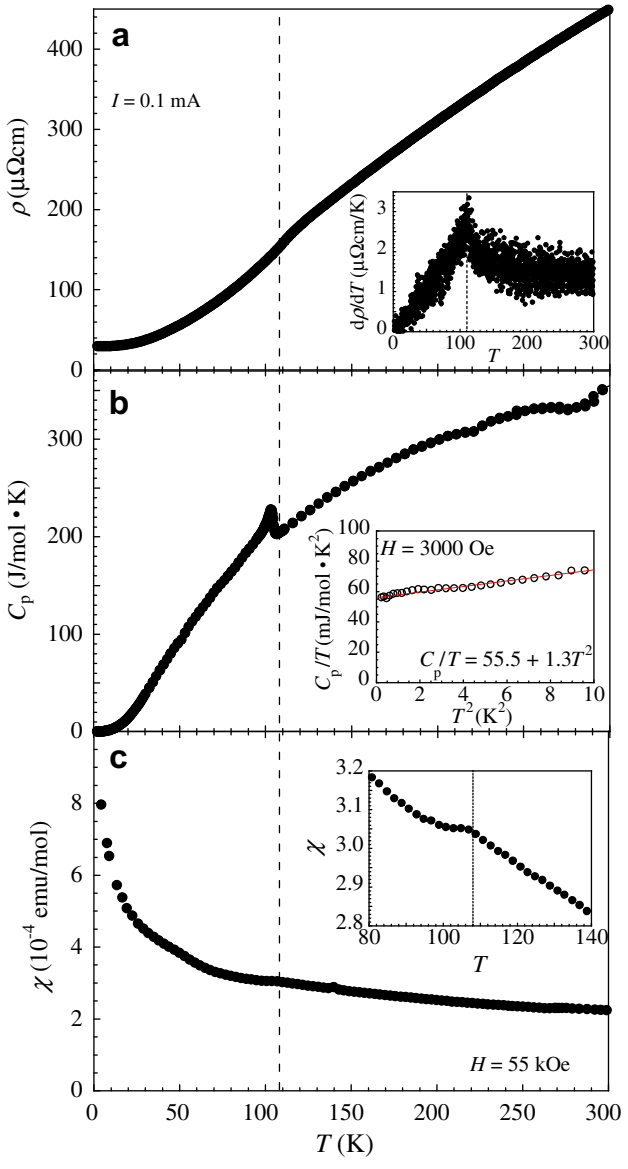

Fig. 2. Temperature dependence of: (a) zero-field electrical resistivity ρ (measuring current $I = 0.1$ mA); (b) zero-field specific heat C_P, and (c) DC susceptibility $\chi_{DC} = M/H$ in an external magnetic field $H = 55$ kOe. In the inset of panel (a) the temperature derivative of the resistivity $d\rho/dT$ as a function of temperature is shown, clearly revealing an anomaly around 110 K. The inset of panel (b) gives the temperature dependence of C_p/T as a function of T^2 in an applied magnetic field $H = 3000$ Oe $> H_{c2}$ representing the normal-state specific heat. The solid line is a fit to the data using Eq. (1). In the inset of panel (c) an extended view of the data for 80 K $\leqslant T \leqslant$ 140 K is presented. The vertical dashed line marks the position of the observed anomaly (110 K) for comparison.

Now we analyze the specific heat in more detail. The entire specific heat at low temperatures consists of electronic and phononic contributions:

$$C_P(T) = C_{el}(T) + C_{ph}(T) = \gamma T + \beta T^3. \quad (1)$$

Applying Eq. (1) to the data in the temperature interval 0.35 K $\leqslant T \leqslant$ 4 K measured at $H = 3000$ Oe $\geqslant H_{c2}$, representing the normal-state specific heat, yields a very good description as shown in the inset of Fig. 2b. From this fit, we deduced the following values for the Sommerfeld coefficient γ and the coefficient of the phononic contribution β: $\gamma = 55.5$ mJ/mol K^2 and $\beta = 1.3$ mJ/mol K^4. Conway et al. [3] reported that their specific-heat data in an applied magnetic DC field $H = 2400$Oe $> H_{c2}$ includes a term proportional to T^{-2} explained by the assumption of paramagnetic impurities contained in their samples. Neither a T^{-2} nor any different term is needed to yield a reasonable description of our data measured in $H =$ 3000 Oe. This gives further evidence that our samples are of a higher quality compared to the samples used in the previous study. The Debye temperature is calculated using the expression $\beta = (12/5)N\pi^4 R\Theta_D^{-3}$ where $N = 18$ denotes the number of atoms per formula unit for $Ag_6O_8AgHF_2$ and $R = 8.314$ J/mol K is the gas constant. Using the fitted value of β, we estimate $\theta_D = 295$ K.

The inverse DC susceptibility exhibits a linear temperature dependence above 110 K. We calculated the effective Bohr magneton $p_{eff} \approx 1.1$ from a linear fit to the data in this temperature range. The kink in the data around 110 K indicates that the magnetic state is affected by the phase transition at 110 K, leading to a possible change of the mixed valences of the Ag ions (in cubic crystal-field symmetry: Ag^+: $4d^{10}$; $S = 0$, Ag^{2+}: $4d^9$; $S = 1/2$, Ag^{3+}: $4d^8$; $S = 1$). Unfortunately, we cannot distinguish between these different states by a bulk magnetization measurement, which is only sensitive to the macroscopic sample average of S rather than the microscopically realized spin states.

3.2. Superconducting properties

Fig. 3 summarizes the resistivity data of three single crystalline samples of $Ag_6O_8AgHF_2$. The onset of superconductivity is indicated by a sharp transition for all three samples (transition width = 0.07 K (sample #1), 0.08 K (sample #2) and 0.05 K (sample #3), respectively). We define T_c as the 50% point of the transition, i.e., where the absolute value of the resistivity has dropped to 50% of the normal-state value.

As seen in Fig. 3, there is a sample dependence of the superconducting transition temperature T_c. To elucidate the origin of this difference, we performed sample growth under different conditions, e.g. changing the synthesis time, the synthesis current, or the concentration of the used HF solution. We determined the values of T_c for seven different single-crystalline samples by resistivity, specific heat, and AC susceptibility measurements, finding $T_c = 1.24$–1.51 K as summarized in Table 1. However, it turned out to be difficult to completely control the sample quality by these parameters. Therefore, we can not resolve this question at the current state of research.

In the superconducting state, the electronic specific heat C_{el} can be obtained by subtracting the phononic term from the total specific heat: $C_{el} = C_P - C_{ph}$. Normalizing the electronic specific heat in the superconducting state to $C_{el}/\gamma T_c$ and plotting the result on a semilogarithmic scale versus T_c/T yields Fig. 4 (sample #5). In the inset, temperature dependence of C_{el} is shown. The solid line in Fig. 4 is an exponential fit to the data in the temperature interval $0.35\ \text{K} \leqslant T \leqslant 0.8\ \text{K}$ using the formula [18]

$$C_{el}/\gamma T_c \propto \exp(-aT_c/T) \tag{2}$$

with $a = \Delta(0)/k_B T_c = 0.94$. From this, we find $\Delta C(T_c)/\gamma T_c \approx 0.67$. On the one hand our specific-heat data seems to vanish exponentially for $T < 0.8$ K as predicted by the BCS theory. On the other hand, the estimated values of $\Delta(0)/k_B T_c$ and the jump height $\Delta C(T_c)/\gamma$ at T_c of the specific heat are much lower than the BCS expectation of 1.76 and 1.43, respectively. However, the superconducting transition causes a very broad anomaly in the temperature dependence of C_P. One might argue again with an affected sample quality due to the exposure to air/moisture, leading to some disorder and inhomogenity and hence causing the broad transition which could also be the reason for the deviation from the BCS expectations for $\Delta(0)/k_B T_c$ and $\Delta C(T_c)/\gamma$. Therefore, it is difficult to speculate about the true gap structure. Here, a specific-heat study down to temperatures below 0.4 K is desirable in order to verify that the specific heat keeps the exponential behavior or not.

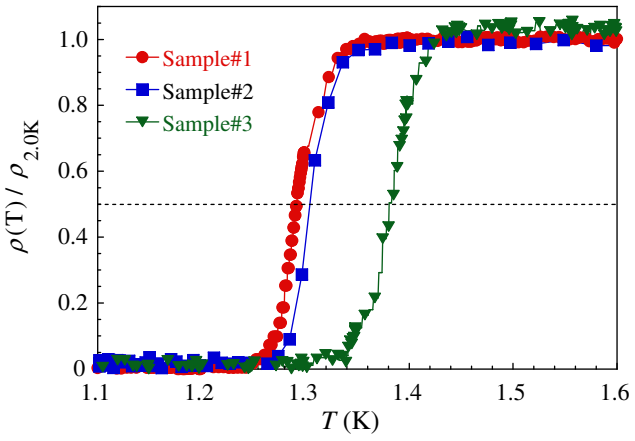

Fig. 3. Electrical resistivity of $Ag_6O_8AgHF_2$. The dashed line indicates, where the resistivity has dropped to 50% of the normal-state value.

Table 1
Sample dependence of the superconducting transition temperature T_c in $Ag_6O_8AgHF_2$: the T_c values of seven different single-crystalline samples were determined by measuring resistivity $\rho(T)$ (samples #1–3), specific heat $C_P(T)$ (#4 and #5), or AC susceptibility $\chi_{AC}(T)$ (#6 and #7) (see text)

Sample	T_c (K)	Quantity
#1	1.30	$\rho(T)$
#2	1.31	$\rho(T)$
#3	1.38	$\rho(T)$
#4	1.24	$C_P(T)$
#5	1.25	$C_P(T)$
#6	1.28	$\chi_{AC}(T)$
#7	1.51	$\chi_{AC}(T)$

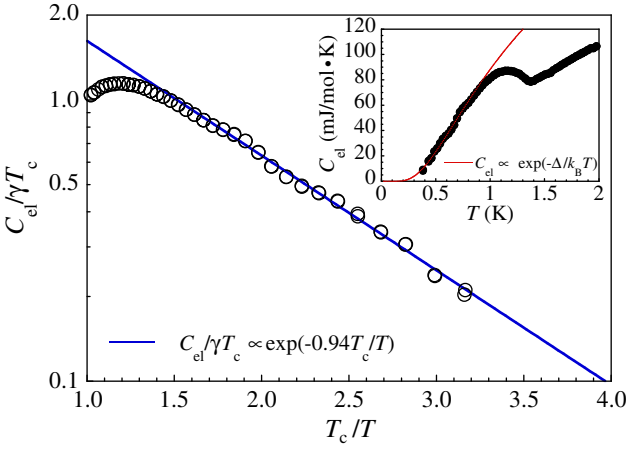

Fig. 4. Normalized electronic specific heat of $Ag_6O_8AgHF_2$ (sample #5) $C_P/\gamma T_c$ in zero field as a function of T_c/T. The solid line is a linear fit to the data. The inset shows the temperature dependence of the electronic contribution to the specific heat C_{el} in zero magnetic field. The solid line is a fit to the data applying the conventional BCS exponential formula (Eq. (2)) (see text).

Fig. 5 shows (a) temperature dependence of the electrical resistivity under magnetic fields up to 2000 Oe and (b) magnetroresistivity as a function of the applied magnetic fields up to 3000 Oe at various temperatures (sample #3) [15]. In these measurements, the DC magnetic field was applied parallel to the measurement current. The resistivity drop indicating the superconducting transition was observed at 1.38 K with a transition width of only 0.05 K.

As before, $T_c(H)$ and $H_{c2}(T)$ are defined as the 50% point of the transition. The critical temperature $T_c(H)$

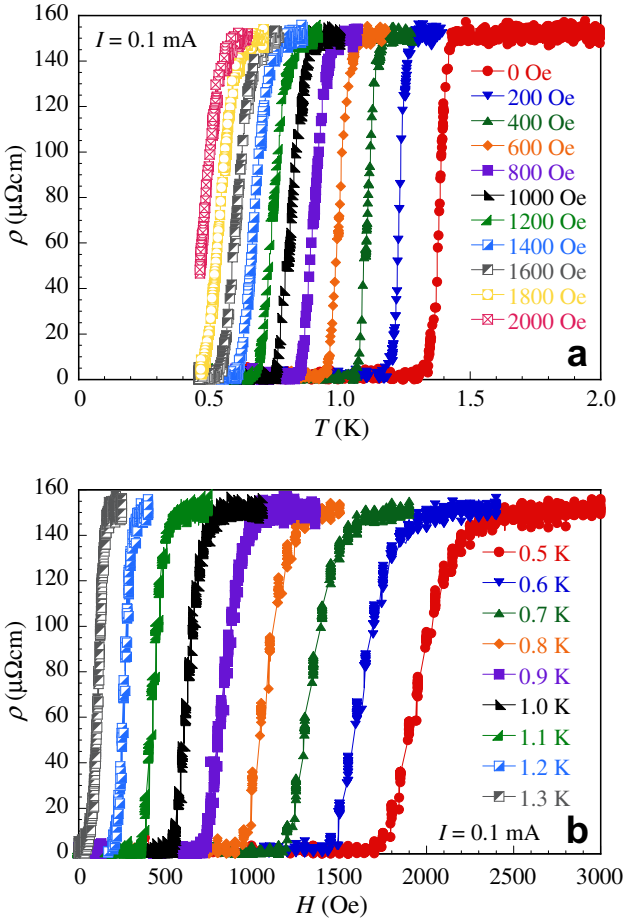

Fig. 5. (a) Temperature dependence of the resistivity in various magnetic fields 0 Oe $\leqslant H \leqslant$ 2000 Oe and (b) magnetroresistivity at various temperatures of $Ag_6O_8AgHF_2$ (sample #3).

(critical field strength $H_{c2}(T)$) is systematically suppressed with increasing magnetic field (temperature); compare Fig. 5a and b, respectively. As is seen in Fig. 5a, the transition width ΔT_c is field independent, indicating that the superconductivity in $Ag_6O_8AgHF_2$ is mean-field like, in clear contrast to low-dimensional superconductors like the high-T_c cuprates, where ΔT_c becomes broader in finite magnetic fields due to fluctuation effects [16].

Fig. 6 summarizes the real part χ' of our AC susceptibility data as a function of temperature in various applied DC-magnetic fields for sample #7, which is the sample with the highest $T_c = 1.51$ K found among our $Ag_6O_8AgHF_2$ samples. The blue curves correspond to the data measured upon decreasing temperature (FC), the red curves to the respective subsequent measurements upon increasing temperature (after FC). The critical temperature $T_c(H)$ is defined as the temperature at which the value of χ' has dropped by 1% of the total shielding $|\Delta\chi'| = |\chi'_{sc} - \chi'_{nc}|$ (sc = superconducting, nc = normal conducting).

The onset of superconductivity and the superconducting volume fraction are systematically suppressed with increasing magnetic field (see Fig. 6). The cooling and warming runs coincide with each other except the data measured

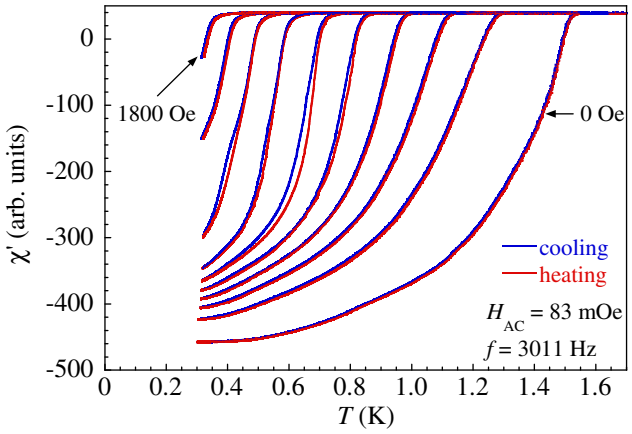

Fig. 6. Temperature dependence of the real part χ' of AC susceptibility in various applied DC magnetic fields 0 Oe $\leqslant H \leqslant$ 1800 Oe for $Ag_6O_8AgHF_2$ (sample #7).

in $H = 1000$ Oe and 1400 Oe. Nevertheless, the onset of superconductivity is non-hysteretic even for these two field strengths and therefore we conclude that $Ag_6O_8AgHF_2$ is a type-II superconductor.

The H–T phase diagram of $Ag_6O_8AgHF_2$ is shown in Fig. 7. The data points are deduced from resistivity and AC susceptibility measurements using samples #3 and #7, respectively. The transition temperature shifts towards lower temperatures as the magnetic field increases. Moreover, the observed sample dependence is reflected in a slight difference between the two phase lines. It remains unclear why the H–T phase line of the sample exhibiting the lower value of T_c (sample #3) features a larger slope than the phase line determined using sample #7.

We note that in the high-T/low-H region of the phase diagram a slope change takes place. The initial curvature of the H–T phase line is concave, becoming linear for intermediate field strengths and changing toward a convex curvature in the low-T/high-H region. Neglecting the slope change just below T_c the gradient of the phase line dH_{c2}/

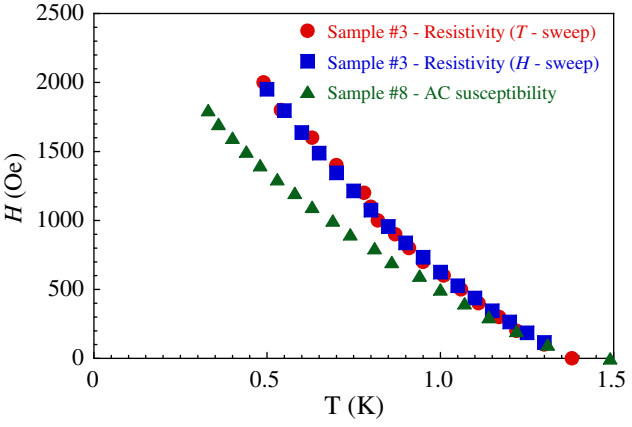

Fig. 7. H–T phase diagram of $Ag_6O_8AgHF_2$ deduced from resistivity (sample #3) and AC susceptibility measurements (sample #7) (compare text).

dT near T_c is estimated to be -2280 Oe/K (resistivity data; sample #3) and -1955 Oe/K (AC susceptibility; sample #7), respectively. Using the standard Wertharmer–Helfand–Hohenberg (WHH) relation [17] $H_{c2} \approx -0.693\,(-dH_{c2}/dT) \times T_c$, we estimate the upper critical field $H_{c2}(0)$ to be 2000–2200 Oe for $Ag_6O_8AgHF_2$. According to the GL-theory for a type-II superconductor, one can estimate the coherence length $\xi(0)$ using the relation $H_{c2} = \Phi_0/2\pi\xi^2$. This yields $\xi(0) = 39$ nm/41 nm for the two specimens.

The upper critical field of $Ag_6O_8AgHF_2$ is clearly below the Pauli-limiting field [19,20] $H_p = 18.4\ \text{kOe/K} \times T_c = 24.8$ kOe. Therefore, we conclude that $Ag_6O_8AgHF_2$ is in an orbital limit and away from the Pauli-limiting regime.

We estimated the thermodynamic critical field $H_c(0)$ on the basis of the relationship:

$$\frac{\mu_0 H_c^2(0)}{2} = -\frac{\gamma}{2}T_c^2 + \int_0^{T_c} C_{el}(T)dT. \tag{3}$$

Thus, from the fit to the specific-heat data using Eq. (3) as shown in the inset of Fig. 4, we obtain a thermodynamic critical field of about $H_c(0) \approx 110$ Oe. The Ginzburg–Landau (GL) parameter κ_{GL} and the magnetic penetration depth $\lambda(0)$ are calculated to be approximately 15 and 560 nm using the relations $H_{c2}(0) = \sqrt{2}\kappa_{GL}H_c(0)$ and $\kappa_{GL} = \lambda(0)/\xi(0)$. The κ_{GL} value is larger than $1/\sqrt{2}$, which divides type-I and type-II superconductors from each other, clearly placing $Ag_6O_8AgHF_2$ into the type-II regime. Using $H_{c1} = H_c/\sqrt{2}\kappa_{GL}$ yields $H_{c1} = 6$ Oe. All estimated parameters are listed in Table 2.

Finally, we compare these results with those obtained for $Ag_6O_8AgNO_3$ [13]. $Ag_6O_8AgNO_3$ undergoes a superconducting transition at $T_c = 1.04$ K and exhibits a Sommerfeld parameter of $\gamma = 46.5$ mJ/mol K^2, which should be compared to $T_c = 1.24$–1.51 K and $\gamma = 55.5$ mJ/mol K^2 for $Ag_6O_8AgHF_2$; see Table 2. In the weak-coupling BCS theory, T_c is given by the equation $k_B T_c = \hbar\omega_{ph}\exp(-1/VN(E_F))$, where ω_{ph} denotes the frequency of the relevant phonons, which is proportional to θ_D, and V is the electron–phonon coupling strength [18]. The different values of T_c possess information on the difference in the density of states at the Fermi level $N(E_F)$ for the two compounds given by

$$\frac{V'}{V} = \frac{\log(T_c/\omega_{ph})}{\log(T_c'/\omega_{ph}')}\frac{N(E_F)}{N'(E_F)}, \tag{4}$$

where we assume $N(E_F)/N'(E_F) = \gamma/\gamma'$. This leads to $V'/V \approx 0.85$ using $T_c = 1.04$ K, $\theta_D = 243$ K, and $\gamma = 46.5$ mJ/mol K^2 for $Ag_6O_8AgNO_3$ and $T_c' = 1.24$–1.51 K, $\theta_D' = 295$K, and $\gamma' = 55.5$ mJ/mol K^2 for $Ag_6O_8AgHF_2$. The T_c value of $Ag_6O_8AgHF_2$ would have been much higher if the electron–phonon coupling strength were not reduced by approximately 15%. An enhancement of $N(E_F)$ may be ascribable to an increased effective mass due to electron–electron and electron–phonon interactions. The lattice constants of $Ag_6O_8AgNO_3$ and $Ag_6O_8AgHF_2$ are 9.893 Å and 9.824 Å, and the ionic radii of NO_3^- and HF_2^- are 1.79 Å and 1.72 Å [21], respectively. If the smaller cage size for the $Ag_6O_8AgHF_2$ leads to a wider band, γ would have been smaller. However the opposite is the case in these compounds. Answering the question which parameter tunes T_c would be a valuable step forward in understanding the superconductivity in the whole family of silver-clathrate superconductors Ag_6O_8AgX.

Table 2
Properties of $Ag_6O_8AgHF_2$ and $Ag_6O_8AgNO_3$ in the normal and superconducting state

	$Ag_6O_8AgHF_2$	$Ag_6O_8AgNO_3$
T_c (K)	1.24–1.51	1.04
H_{c1} (Oe)	6	22
H_{c2} (Oe)	2000–2200	770
H_c (Oe)	110	130
$\lambda(0)$ (nm)	560	270
$\xi(0)$ (nm)	39–41	66
κ_{GL}	15	4.2
$\Delta C/\gamma T_c$	0.67	0.94
$2\Delta/k_B T_c$	1.88	2.36
γ (mJ/mol K^2)	55.5	46.5
β (mJ/mol K^4)	1.3	2.6
θ_D (K)	295	243

4. Summary

In this paper, we discuss normal-state and superconducting properties of $Ag_6O_8AgHF_2$ by means of electrical resistivity, specific heat, and DC and AC susceptibility data using single crystalline samples.

In the normal-state, we found a phase transition around 110 K indicated by anomalies in ρ, C_P, and χ_{DC}. The origin remains unclear. However, the fact, that a similar anomaly caused by a structural phase transition takes place around 185 K in the closely related compound $Ag_6O_8AgNO_3$ [13] suggests that $Ag_6O_8AgHF_2$ also undergoes a structural phase transition.

From the specific-heat measurement, we estimated the parameters γ, β, and θ_D to be 55.5 mJ/mol K^2, 1.3 mJ/mol K^4, and 295 K, respectively.

From our analysis of the superconducting state, we found that $Ag_6O_8AgHF_2$ is a bulk type-II superconductor. We observed a sample dependent transition temperature $T_c \approx 1.24$–1.51 K and an upper critical field strength $H_{c2}(0) \approx 2000$–2200 Oe. We calculated the basic superconducting parameters as summarized in Table 2: The coherence length amounts to $\xi(0) \approx 40$ nm, the Ginzburg–Landau parameter to $\kappa_{GL} \approx 15$, and the penetration depth to $\lambda(0) \approx 560$ nm, respectively.

An analysis of the specific-heat data below T_c in the framework of the BCS theory yields $\Delta C/\gamma T_c = 0.67$ and $\Delta/k_B T_c = 0.94$ which are clearly smaller than the prediction of the BCS theory. However, due to the broadness of the transition, it is difficult to judge whether the estimated values are intrinsic or not. Therefore, further studies are required to determine the true nature of the superconduc-

ting gap, e.g. specific-heat experiments at a lower temperature scale.

From a comparison with $Ag_6O_8AgNO_3$, electron–phonon coupling strength is reduced by changing the X site ion from NO_3^- to HF_2^-. To further clarify this point, a comprehensive substituent-dependent investigation of the crystal structure of Ag_6O_8AgX with e.g. $X = NO_3^-$, HF_2^-, HCO_3^-, and other substituents, is desirable.

Acknowledgements

This work was partially supported by a Grant-in-Aid for Science Research from the Ministry of Education, Culture, Sports, Science and Technology, Japan, and Grant-in-Aid for JSPS Fellows. M.K. is supported by MEXT.

References

[1] M.B. Robin, K. Andres, T.H. Geballe, N.A. Kuebler, D.B. McWhan, Phys. Rev. Lett. 17 (1966) 917.
[2] A.C. Gossard, D.K. Hindermann, M.B. Robin, N.A. Kuebler, T.H. Geballe, J. Am. Chem. Soc. 89 (1967) 7121.
[3] M.M. Conway, N.E. Phillips, T.H. Gebelle, N.A. Kuebler, J. Phys. Chem. Solids 31 (1970) 2673.
[4] J. Selbin, M. Usategui, J. Inorg. Nucl. Chem. 20 (1961) 91.
[5] M. Jansen, S. Vensky, Z. Naturforsch. 55b (2000) 882.
[6] U. Bilow, M. Jansen, Z. Naturforsch. 50b (1995) 990.
[7] M. Jansen, U. Bilow, J. Alloys Compd. 183 (1992) 45.
[8] C.H. Wong, T.H. Lu, C.N. Chen, T.J. Lee, J. Inorg. Nucl. Chem. 34 (1972) 3253.
[9] I. Náray-Szabó, G. Argay, P. Szabó, Acta Cryst. 19 (1965) 180.
[10] I. Náray-Szabó, K. Popp, Z. Anorg. Allg. Chem. 322 (1963) 286.
[11] J.A. McMillan, Chem. Rev. 62 (1962) 65.
[12] K. Momma, F. Izumi, Commission on Crystallogr. Comput., IUCr Newslett. 7 (2006) 106.
[13] K. Kawashima, M. Ishii, H. Okabe, J. Akimitsu, M. Kriener, H. Takatsu, S. Yonezawa, Y. Maeno, J. Phys. Soc. Jpn. 77 (2008) 024707.
[14] E. Torikai, E. Maeda, Y. Kawami, Nippon kagaku zasshi 91 (1970) 87 (in Japanese).
[15] The results shown in Fig. 2a and Fig. 5 were obtained by using two different samples which explains the difference in the residual resistivity values in the two plots.
[16] W.K. Kwok, J.A. Fendrich, C.J. van der Beek, G.W. Carbtree, Phys. Rev. Lett. 73 (1994) 2614.
[17] N.R. Werthamer, E. Helfand, P.C. Hohenberg, Phys. Rev. 147 (1966) 295.
[18] M. Tinkham, Introduction to Superconductivity, Dover Publications, New York, 1996.
[19] K. Maki, Phys. Rev. 148 (1966) 362.
[20] A.M. Clogston, Phys. Rev. Lett. 9 (1962) 266.
[21] R.D. Shannon, Acta Cryst. A32 (1976) 751.